JACS
JOURNAL OF THE AMERICAN CHEMICAL SOCIETY

Article

pubs.acs.org/JACS

Aggregation in a High-Mobility n-Type Low-Bandgap Copolymer with Implications on Semicrystalline Morphology

Robert Steyrleuthner,[†] Marcel Schubert,[†] Ian Howard,[§] Bastian Klaumünzer,[‡] Kristian Schilling,[⊥] Zhihua Chen,[∥] Peter Saalfrank,[‡] Frédéric Laquai,[§] Antonio Facchetti,[∥] and Dieter Neher*[,†]

[†]Institute of Physics and Astronomy and [‡]Institute of Chemistry, University of Potsdam, D-14476 Potsdam, Germany

[§]Max Planck Institute for Polymer Research, D-55021 Mainz, Germany

[⊥]Nanolytics GmbH, D-14476 Potsdam, Germany

[∥]Polyera Corporation, Skokie, Illinois 60077, United States

Supporting Information

ABSTRACT: We explore the photophysics of P(NDI2OD-T2), a high-mobility and air-stable n-type donor/acceptor polymer. Detailed steady-state UV−vis and photoluminescence (PL) measurements on solutions of P(NDI2OD-T2) reveal distinct signatures of aggregation. By performing quantum chemical calculations, we can assign these spectral features to unaggregated and stacked polymer chains. NMR measurements independently confirm the aggregation phenomena of P(NDI2OD-T2) in solution. The detailed analysis of the optical spectra shows that aggregation is a two-step process with different types of aggregates, which we confirm by time-dependent PL measurements. Analytical ultracentrifugation measurements suggest that aggregation takes place within the single polymer chain upon coiling. By transferring these results to thin P(NDI2OD-T2) films, we can conclude that film formation is mainly governed by the chain collapse, leading in general to a high aggregate content of ∼45%. This process also inhibits the formation of amorphous and disordered P(NDI2OD-T2) films.

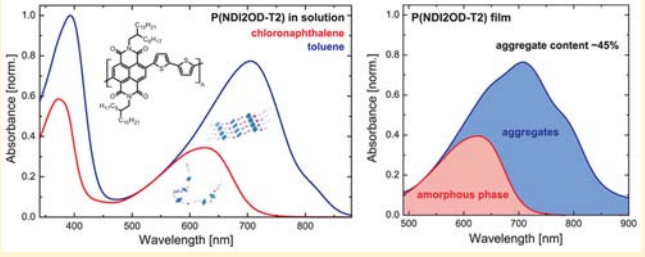

INTRODUCTION

Structural elucidation has emerged as a substantial topic in the field of today's soft matter physics. Understanding the relation between form and function of biomolecules like proteins and nucleic acids is at the core of biochemical research. Equivalent effort is underway to accurately understand the structure of synthetic organic macromolecules designed for functional electronic devices, such as organic solar cells (OSCs), organic light-emitting diodes (OLEDs), and organic field-effect transistors (OFETs).[1] From these studies, it was found that certain synthetic π-conjugated polymers tend to adopt numerous nonplanar conformations, resulting in disordered films with poor interchain order. On the other hand, strong intermolecular interactions between functional units (e.g., side chains) or the aromatic rings in the backbone of conjugated polymers ($\pi-\pi$ stacking) can lead to local ordering phenomena. These competing processes can induce a strong dependency of the material microstructure in a thin film on the preparation conditions. Besides the challenge of controlling and characterizing the semiconductor microstructure, a detailed understanding of its influence on device performance is essential. It is well documented that the charge transport properties of conjugated polymers are severely influenced by the microstructure of the semiconducting layer.[2−9] For example, Rivnay et al. proposed that structural imperfections in semicrystalline conjugated polymers can induce additional states within the bandgap that act as traps and consequently reduce the mobility.[10] However, regular close packing of the polymer chains not only will reduce the width of the density of tail state distributions but also can enhance the overlap of π electron orbitals, increasing the transfer integral for charge hopping dramatically.

In 2009, Facchetti and co-workers reported a novel n-type polymer, P(NDI2OD-T2) (also known as Polyera ActivInk N2200), that exhibited a large electron field-effect mobility of up to 0.85 cm^2/Vs.[11] A series of publications followed, shedding light on the injection and transport of charges,[12−17] energetic disorder,[18−20] and film morphology or texture.[21−25] By combining time-of-flight and single-carrier device measurements, we could show that the bulk transport in P(NDI2OD-T2) perpendicular to the layer plane is trap-free and likewise outstanding, with mobility values above 10^{-3} cm^2/Vs.[12] A narrow distribution of transport states was later deduced from Kelvin probe studies[18] and temperature-dependent OFET measurements.[19] The polymer was further applied as the electron-accepting component in OSCs, though with rather low power conversion efficiencies.[25−29] Based on the results reported in this study, we were recently able to achieve an increased power conversion efficiency of 1.4% for a poly(3-

Received: July 13, 2012
Published: September 10, 2012

   dx.doi.org/10.1021/ja306844f | J. Am. Chem. Soc. 2012, 134, 18303−18317

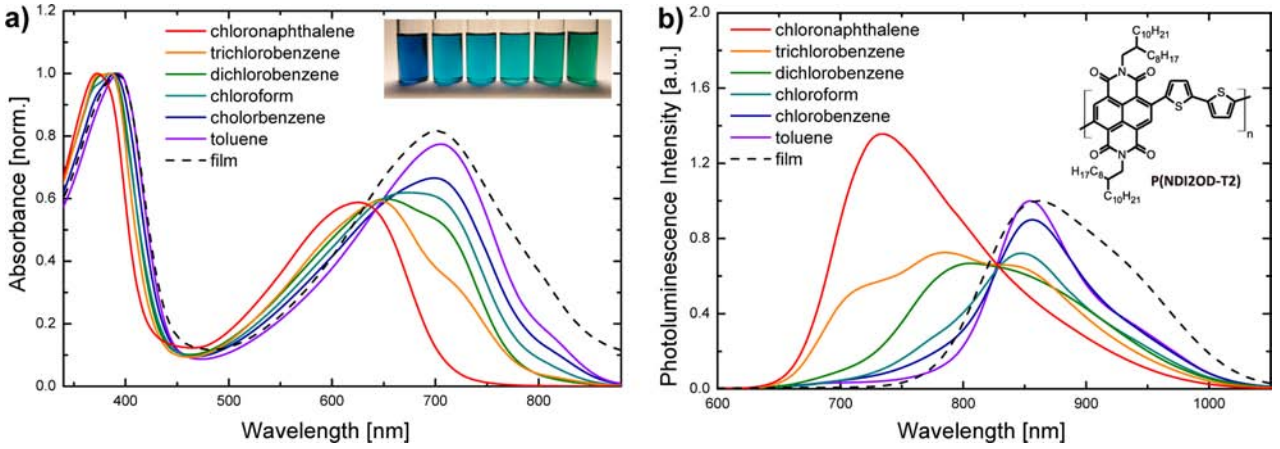

Figure 1. (a) Absorption and (b) fluorescence spectra of P(NDI2OD-T2) in various solvents at a concentration of 1 g/L. The photoluminescence spectra were recorded for an excitation wavelength of 560 nm. Film spectra are also displayed for comparison. The inset in panel a shows a photograph of the solutions under investigation (with CN on the left to toluene on the right). The chemical structure of P(NDI2OD-T2) is shown in the inset of panel b.

hexylthiophene) (P3HT):P(NDI2OD-T2) bulk heterojunction solar cell, with a remarkable fill factor of 70%.[30]

While it was initially believed that layers from P(NDI2OD-T2) are mostly amorphous,[11] grazing incidence X-ray diffraction (GIXD) studies by Rivnay et al. on P(NDI2OD-T2) layers showed an exceptional in-plane order with distinct "π-stacking" of the naphthalene diimide (NDI) cores.[21] In fact, rylene dyes have been the focus of scientific investigation and commercial application for decades. Their optical properties can be widely tuned, e.g., by changing the solubilizing substituents. This behavior is commonly explained by different types of aggregates that are formed by these planar dye molecules, depending on their specific chemical structure.[31−37] If this strong tendency to form aggregates or supramolecular structures is preserved in the rylene-containing copolymer, intermolecular interactions should largely determine the morphology and consequently the optical and electrical properties of P(NDI2OD-T2). However, a more recent study by Schuettfort et al., combining GIXD and near-edge X-ray absorption fine structure, indicated that a significant proportion of polymer chains are contained in amorphous areas, both in the near-surface regions and in the bulk of the film.[22] These authors also compared the OFET properties of P(NDI2OD-T2) layers annealed at 220 and 320 °C followed by rapid cooling. While the former layer exhibited well-resolved diffraction peaks in GIXD studies, the sample cooled from 320 °C (above the melting temperature, T_m) appeared to be quite amorphous. Despite these structural differences, these layers had rather similar mobilities, differing by a factor less than 3. The authors concluded that the high mobility of P(NDI2OD-T2) is not simply related to high structural order in the film. Quantifying the absolute crystalline amount can significantly enhance the understanding of the outstanding performance of this material.

We approach this issue through a detailed spectroscopic study of P(NDI2OD-T2). Our approach is motivated by the detailed understanding of chain aggregation in P3HT in solution and solid state based on optical spectroscopy.[38,39] It is well established that the optical absorption of P3HT in a good solvent exhibits a broad and featureless absorption, while aggregation of the polymer chains induces an additional low-energy vibronic progression.[40] A model of weakly interacting H-aggregates developed by Spano has been successfully applied to analyze the optical absorption properties of P3HT layers with regard to their nanostructure and crystallinity.[41,42] Information gained from these studies for films cast from various solvents or on fractions of different molecular weight could be well correlated with hole transport properties.[43] Spectral signatures of aggregation have also been investigated for other conjugated polymers like polyphenylene vinylene[44−51] or polyfluorene derivates.[52−54] On the other hand, detailed investigations on the spectroscopic changes upon aggregation are very rare for low-bandgap copolymers. Notably, a red-shift of the low-energy absorption in high-performance OSCs comprising such polymers is commonly ascribed to an increased interaction of the chains and a higher degree of crystallinity.[55−61]

EXPERIMENTAL SECTION

P(NDI2OD-T2) of different molecular weights (M_w) was synthesized according to a modified procedure.[29] The M_w was determined by a Waters gel permeation chromatography (GPC) system (Waters pump 510) in chloroform (CF) at room temperature vs polystyrene standards. The M_w and polydispersity index (PDI) of the conventional P(NDI2OD-T2) (mid-M_w batch in this study) were found to be 181 kDa and 5.0, respectively, and it was synthesized by reacting NDI2OD-Br2 (1.10 equiv) with 5,5′-bis(trimethylstannyl)-2,2′-bithiophene (1.00 equiv) using the conditions of ref 29. Under similar synthetic conditions but using a stoichiometric amount of the two monomers (at a ratio of 1.00 equiv/1.00 equiv), a high-molecular-weight P(NDI2OD-T2) batch was obtained with M_w = 1105 kDa and PDI = 2.1. The low-molecular-weight P(NDI2OD-T2) batch, with M_w = 118 kDa and PDI = 4.0, was obtained by concentrating the filtrate of the precipitation of the mid-weight polymer:CF solution in a mixture of THF and methanol (2:1, v/v). All solvents used in this study were obtained from Sigma Aldrich and used as received.

Information about the methods used for the preparation of polymer solutions and films and the measurement techniques employed in this study can be found in the Supporting Information.

RESULTS

Absorption and Fluorescence in Different Solvents. Figure 1a shows UV−vis absorption and near-infrared (NIR) fluorescence spectra of P(NDI2OD-T2) dissolved in a variety of common solvents at a concentration of 1 g/L (corresponding to a molar concentration of the repeat units of 10^{-3} mol/L).

dx.doi.org/10.1021/ja306844f | J. Am. Chem. Soc. 2012, 134, 18303−18317

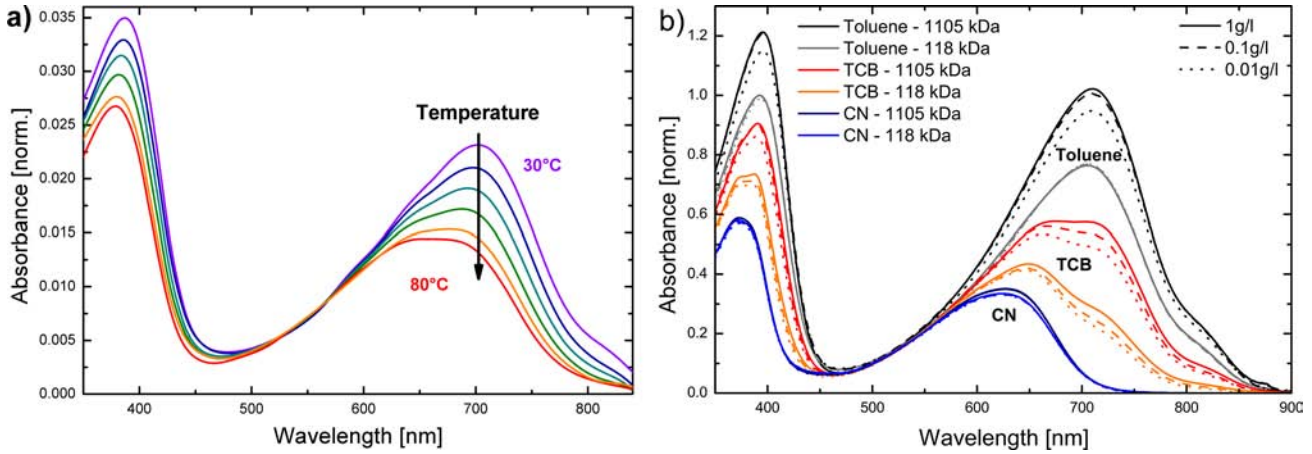

Figure 2. (a) Absorption of P(NDI2OD-T2) with a nominal M_w = 181 kDa in toluene at a concentration of 0.001 g/L for different temperatures. (b) Absorption spectra of two fractions (M_w = 118 and 1105 kDa) of P(NDI2OD-T2) in toluene, trichlorobenzene (TCB), and chloronaphthalene (CN) at three different concentrations. The absorption spectra are normalized to the absorbance at 550 nm.

As for other copolymers comprising donor and acceptor units, the absorption spectrum of P(NDI2OD-T2) in any solvent is characterized by two spectral features, a high-energy peak attributed to the $\pi-\pi^*$ transition and a broad, low-energy band ascribed to the charge-transfer (CT) transition that evolves significant redistribution of electrons from the donor moiety to the acceptor unit along the main chain.[62] In toluene or chlorobenzene, the absorption spectrum extends into the red to NIR, with a peak at 710 nm and a shoulder at ~800 nm. The spectra of these solutions roughly resemble the absorption of P(NDI2OD-T2) in the solid state. In contrast, the absorption of the polymer in chloronaphthalene (CN) lacks these low-energy features, and the spectrum in the visible is determined by a broad and featureless band centered at 620 nm.

Similar spectral changes are seen in the fluorescence spectra of P(NDI2OD-T2) shown in Figure 1b. As for the absorption, going from CN to toluene leads to a pronounced red-shift of the emission maximum. The photoluminescence (PL) in CN is characterized by a single band with a maximum at 720 nm and a broad tail extending to 1000 nm. The spectrum in toluene, on the other hand, exhibits a rather structured emission, with the maximum at 860 nm and a second peak at ~950 nm. Again, the emission in toluene exhibits spectral features similar to those seen in thin solid films. Therefore, we propose that aggregated chain segments dominate the emission of P(NDI2OD-T2) in toluene at a concentration of 1 g/L. The emission spectra in the other solvents are rather complex. At the first sight, these spectra cannot be described by a simple superposition of the emission spectra in CN and toluene. Noticeably, the PL spectrum in trichlorobenzene (TCB) shows distinct peaks at 720, 780, and 860 nm, and these features also seem to contribute to the PL measured in dichlorobenzene (DCB).

Solvatochromism is a well-known effect, where the absorption of a chromophore strongly depends on the choice of solvent.[63,64] For molecules that exhibit unequal dipole moments in the ground and excited states, solvatochroism is caused by electrostatic interactions with the surrounding solvent molecules. In this case, the absorption bands move continuously to higher (or lower) wavelengths depending on the polarity of the solvent. At a first glance the observed absorbance shifts in Figure 1 seem to correlate with the polarities of the chosen solvents (except for CF; see Supporting Information for table). However, there is solid experimental evidence that the distinct optical properties of P(NDI2OD-T2) in different solvents are primarily caused by chain aggregation, that the absorption and fluorescence in CN can be attributed to nonaggregated chains, and that a large fraction of chain segments is aggregated in toluene solution. Three key observations support this conclusion:

(a) Fluorescence excitation spectra in CN measured for emission at 710, 770, and 830 nm are identical and follow exactly the absorption (Figure S1a). This means that the entire emission is caused by a single absorbing species, which is the nonaggregated chain. On the other hand, excitation spectra of P(NDI2OD-T2) in toluene vary significantly when the emission wavelength is shifted to the red. This is clearly seen in Figure S1b, suggesting that the polymer in toluene exists in at least two distinct states with characteristic absorption and emission.

(b) Raising the temperature induces a continuous decrease of the long-wavelength absorption features (at 710 and 810 nm) for P(NDI2OD-T2) in toluene, while it does not affect the positions of the absorption bands (Figure 2a). This is consistent with increased solubility for a higher solvent temperature, decreasing the fraction of polymer in an aggregated state.

(c) The absorption has a significant dependence on polymer M_w (Figure 2b). Similar effects have recently been reported for P3HT fractions of different molecular length.[65] The absorption spectra of these fractions could be separated into contributions from non-aggregated and aggregated chains, with higher M_w causing a higher percentage of chains to form aggregates at a given concentration.

On the other hand, changing the P(NDI2OD-T2) concentration does not alter the absorption significantly (Figure 2b), though higher concentrations will potentially increase the likeliness of intermolecular aggregation. We therefore conclude that varying degrees of chromophore aggregation, as evidenced by prominent changes in absorption and emission, are intrachain phenomena and related to different conformations of individual chains (depending on the quality of the solvents). This is different for the soluble poly(*p*-phenylene vinylene) derivative MEH-PPV, where distinct optical changes

dx.doi.org/10.1021/ja306844f | J. Am. Chem. Soc. 2012, 134, 18303−18317

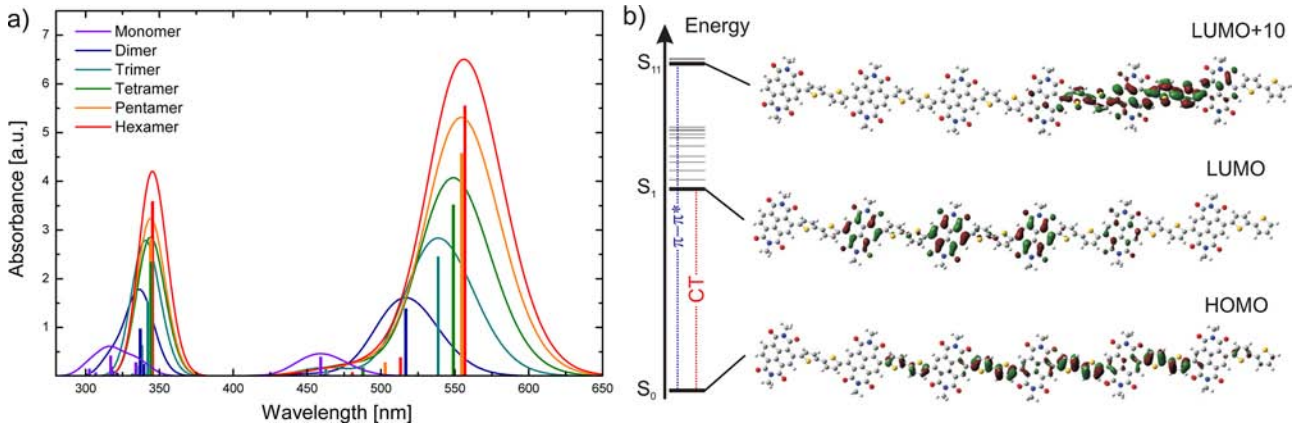

Figure 3. (a) Calculated vertical transition energies for a series of P(NDI2OD-T2) oligomers (vertical lines), broadened in energy by σ = 100 meV (lines). (b) HOMO, LUMO, and LUMO+10 which mainly contribute to $\pi-\pi^*$ and CT transitions, calculated for the hexamer with CAM-B3LYP/SVP.

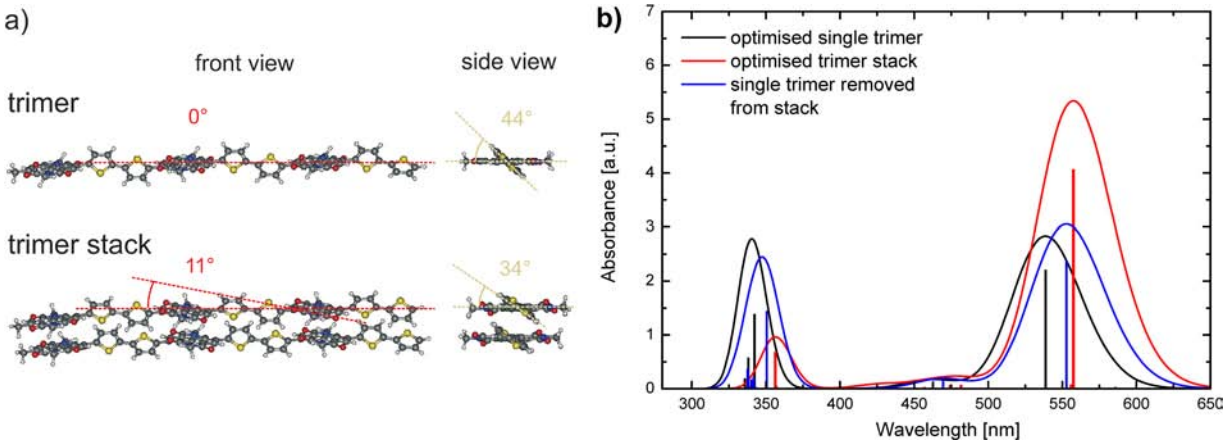

Figure 4. (a) DFT-optimized structures of a single P(NDI2OD-T2) trimer and a trimer stack. Red lines indicate the tilt of the NDI units, while yellow lines illustrate the planarization of thiophene rings upon stacking. (b) Corresponding calculated vertical transition energies.

in absorption were attributed to a conformational transition driven by both intrachain and interchain interactions.[66]

Quantum Chemical Calculations. Insight into the intrinsic photophysics of isolated P(NDI2OD-T2) can be gained by quantum chemical (QC) density functional theory (DFT) calculations. As computational costs increase polynomially with increasing oligomer length, conclusions on the photophysics of polymers are typically drawn via the oligomer approach.[67] A more recent review devoted to QC calculations on low-bandgap polymers[68] shows that DFT is capable of providing an accurate description of the photophysics of donor/acceptor copolymers designed for application in OSCs.[62,69−89]

We used DFT to calculate the vertical transition energies for a series of oligomers from monomer to hexamer. The ground-state geometries, as shown for the hexamer in Figure 3b, were optimized for all oligomers with the B3LYP functional[90,91] and the SVP[92,93] basis set as implemented in TURBOMOLE6.3.[94] Absorption spectra were calculated with TD-CAM-B3LYP,[95] within the GAUSSIAN09 program package,[96] since it has proven to be a suitable DFT functional for CT transitions.[97] The discrete transition energies have been broadened by a Gaussian distribution with σ = 100 meV. The calculated spectra as shown in Figure 3a generally resemble the shape of the measured spectra, with the high-energy $\pi-\pi^*$ transition and the low-energy CT transition. The TD-DFT calculations also reveal additional states with negligible oscillator strength, which will not be discussed in the following. As the chain length is increased, the excited states become more delocalized, resulting in a red-shift of both transitions. The energy of the CT transition converges rapidly with increasing chain length, and at convergence the transition energy is only 0.2 eV higher than the energy of maximum absorbance in CN, where in solution no additional vibronic structure is observed. A detailed TD-DFT benchmark study on an extended set of molecules revealed that CAM-B3LYP delivers transition energies with a mean absolute error of ~0.25 eV.[98] Within the accuracy and capability of this QC approach, and considering also that the hexamer might be below the polymer limit, the measured absorbance in CN is consistent with the predictions for electronic transitions on nonaggregated free P(NDI2OD-T2) chains, strongly supporting the assignment we made in the previous section.

In addition, optimization of the ground-state geometry and calculation of the transition energies have been performed for the trimer in different solvents (see Supporting Information). These calculations showed only a small shift of the absorbance, depending on the solvent polarity. This finding is in full support of our interpretation that chain collapse and "chromophore"

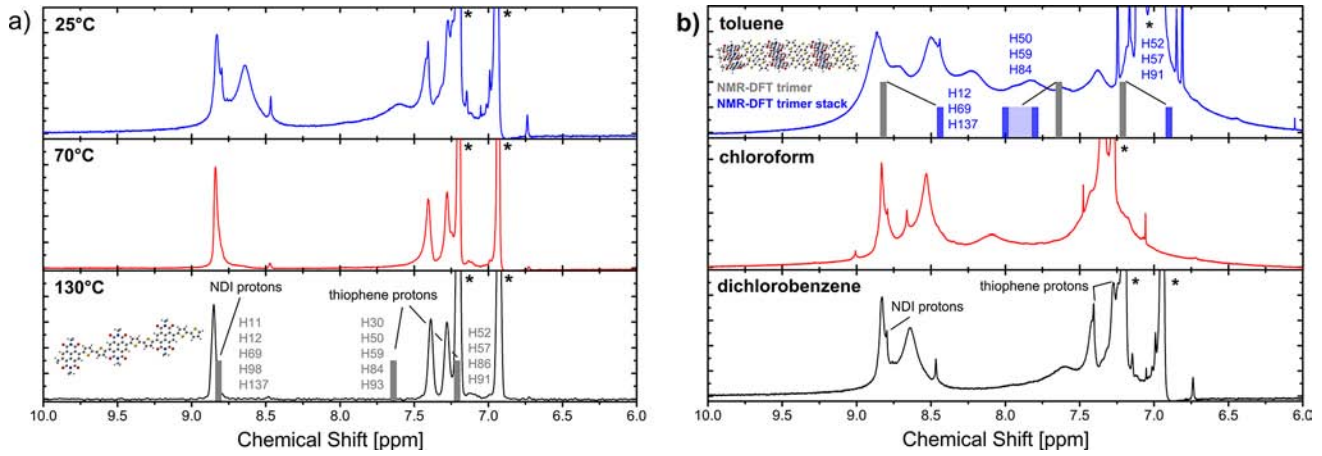

Figure 5. NMR spectra of P(NDI2OD-T2) (a) in deuterated dichlorobenzene measured at 130 °C, 70 °C, and room temperature and (b) in deuterated dichlorobenzene, chloroform, and toluene at room temperature (concentration 15 g/L). Apparent solvent peaks are indicated by an asterisk. The graphs also show NMR-DFT (B3LYP/SVP) calculations for a P(NDI2OD-T2) trimer (gray bars) and the central trimer in a stack (blue bars). The structures and assignments to the atom numbers can be found in the Supporting Information.

aggregation rather than polarisation effects explain the solvent dependence of optical properties.

Figure 3b also shows pictures of the HOMO, LUMO, and LUMO+10 for the hexamer in vacuum. While the HOMO is mainly localized on the dithiophene unit, the LUMO is located on the NDI. This again underlines the distinct CT character of the main electronic transition of this conjugated polymer. The strong localization of the frontier orbitals also suggests that charge transport may be very efficient between coplanar and closely spaced NDI units of adjacent chains.[69] Consequently, electron transport in P(NDI2OD-T2) should be considerably influenced by thin-film morphology and spatial arrangement of neighboring NDI units, in the direction perpendicular to the chain backbone.

We note that Caironi et al. calculated optical transitions of P(NDI2OD-T2) via the semiempirical ZINDO method[19] and in a subsequent paper Fazzi et al. also applied DFT (various functionals were used, and the 6-31G* basis was implied).[20] The $\pi-\pi^*$ and CT transitions were well described in both cases. Nevertheless, caution should still be exercised in making comparisons with experimental data, as all the different theoretical approaches so far have not considered the influence of intermolecular states on the absorption spectrum, which clearly can be important for this polymer.

To address the effect of intermolecular interactions on the absorption spectrum, we performed geometrical optimization of a P(NDI2OD-T2) trimer stack. The trimer stack was optimized with B3LYP/SVP with dispersion correction (DFT-D2)[99] as implemented in TURBMOLE6.3. In agreement with DFT calculations by Schuettfort et al.,[22] our optimized stacks of P(NDI2OD-T2) oligomers exhibit a close proximity of the NDI units in the stack (Figure 4a), suggesting a favorable structure for interchain electron transport. Furthermore, distinct changes in the oligomer conformation occur. In comparison to a single trimer, the planar NDI units tilt out of the polymer plane by 11°, while the side view demonstrates a reduction of the thiophene twist angle from 44° to 34°. Figure 4b shows the calculated UV–vis absorption spectra of these two structures (black and red curves). Upon stacking, the CT transition is red-shifted by 80 meV. In order to distinguish whether this shift in mainly caused by a conformational change or by additional electronic interactions between adjacent chains, we separated one trimer from the stack and calculated the absorption without further geometry optimization (blue curve). This comparison clearly suggests that the main contribution to the red-shift of the absorption is a change in conformation of the oligomer upon stacking. This behavior is in fact very comparable to the spectral changes of polythiophenes upon aggregation. Detailed studies on the thermochroism of polythiophenes could identify the planarization of the chains as the main conformational change, leading to an increased conjugation length and shifting the absorption to longer wavelengths.[100−105]

Thus, our DFT calculations suggest that the absorbance seen in CN is caused by intrachain excitons on isolated P(NDI2OD-T2) chains. Conformational changes upon aggregation are proposed as the main reason for the red-shifted absorption.

Nuclear Magnetic Resonance in Solutions. In this section, we provide further evidence for the aggregation of P(NDI2OD-T2) in solution, independent of optical spectroscopy. Nuclear magnetic resonance (NMR) spectroscopy probes the local electronic environment of an atom with nonzero nuclear spin. For this reason, NMR spectroscopy is not only applied to the identification of molecules but also utilized complementary to X-ray crystallography for structural analysis of proteins or nucleic acid fragments[106−109] and self-organization processes of small synthetic molecules.[37,110,111] Recently ^{1}H NMR spectroscopy was employed to resolve the aggregation mechanisms and structures of polyfluorene and poly(*p*-phenylene vinylene) derivatives in solution.[112−115] In addition, solid-state NMR spectroscopy was used to obtain detailed knowledge about the correlation between thermochroism and molecular structure of polythiophenes.[116,117] Moreover, solid-state NMR was applied to understand the exact stacking of and interaction between neighboring polymer chains of a novel donor/acceptor copolymer.[118] In order to check the molecular arrangement of P(NDI2OD-T2) stacks suggested by DFT geometry optimization, we combined ^{1}H NMR spectroscopy on solutions of varying solvent quality with theoretical calculations on the expected chemical shifts.

Figure 5a shows the ^{1}H NMR spectra of P(NDI2OD-T2) in deuterated DCB at 130 °C, 70 °C, and room temperature. Our investigation is focused on the chemical shift of protons attached to the aromatic rings (thiophene and the NDI core

dx.doi.org/10.1021/ja306844f | J. Am. Chem. Soc. 2012, 134, 18303−18317

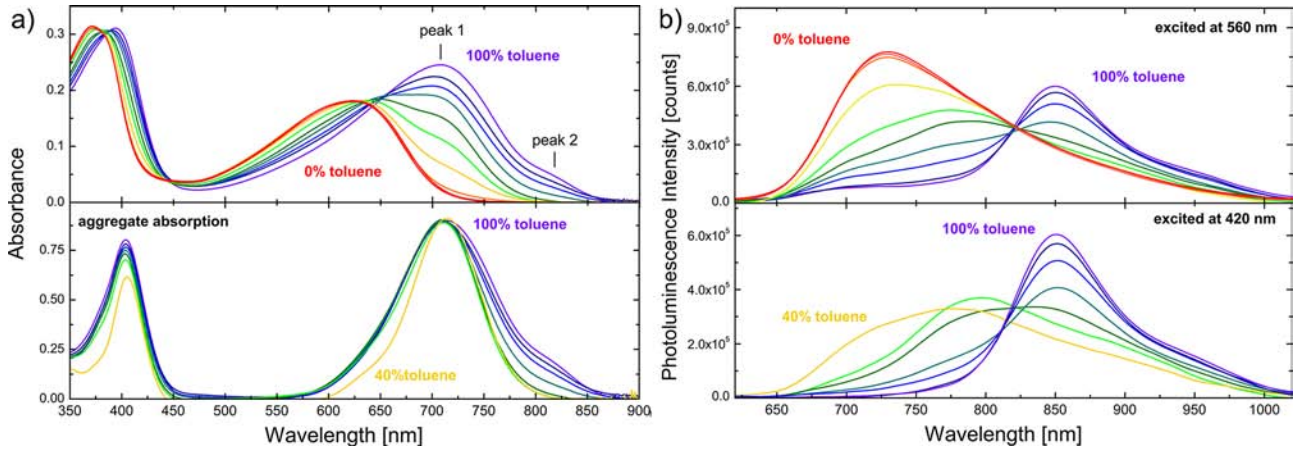

Figure 6. (a) Absorbance and (b) fluorescence spectra of P(NDI2OD-T2) in toluene:CN mixtures at a concentration of 0.1 g/L. The PL spectra were recorded for excitation wavelengths of 560 (top) and 420 nm (bottom). The bottom of panel a also shows the aggregate absorption obtained by subtraction of the 0% toluene spectrum.

protons), since $\pi-\pi$ stacking directly leads to shielding/deshielding due to induced aromatic ring currents of the neighboring molecules.[119−123] From the previous UV−vis analysis, DCB can be considered as a tolerably good solvent for this material. Nevertheless, clear resolution of the three aromatic peaks is reached only at a high temperature of 130 °C. Furthermore, Figure 5b shows the ^{1}H NMR spectra in CF and toluene at room temperature, with distinct new peaks appearing. This effect is indicative for the formation of an additional chemical environment. Broadening of the peaks is observed upon decreasing solvent quality. Here we will focus on the appearance of new chemical shifts, while the origin of this broadening will be discussed in a subsequent study.

A detailed understanding of the ^{1}H NMR spectra can be obtained by comparison with theoretical predictions on the chemical shifts based on DFT calculations. ^{1}H NMR shielding tensors are computed with the Gauge-Independent Atomic Orbital (GIAO) method[124] as implemented in Gaussian 09.[96] Here B3LYP/SVP was again used for the theoretical method. The NMR shieldings were referenced to tetramethylsilane. Figure 5a shows the calculated chemical shifts of the aromatic protons for a P(NDI2OD-T2) trimer. The calculated shifts for a single trimer are in good agreement with experimental data in high-temperature DCB, and therefore this is taken as the NMR spectrum of nonaggregated P(NDI2OD-T2). The experimental peak at 8.85 ppm can be clearly assigned to protons attached to the NDI unit, while the peaks at 7.38 and 7.28 ppm correspond to thiophene protons. Upon aggregation, these protons experience shielding/deshielding by the nearby conjugated systems, which leads to the appearance of new chemical shifts. In order to simulate the effect of stacking on the NMR spectra, we used the geometrically optimized trimer stack presented in the previous section. Edge effects were reduced by placing a third trimer on top of the stack, using the geometric displacement of the NDI units in the optimized stack. Figure 5b shows the calculated ^{1}H NMR chemical shifts for the central trimer of the stack. NDI protons (H12, H69, H137) experience significant shielding equivalent to a clear upfield shift of the peak by 0.38 ppm. In fact, experimental spectra show a very strong peak at this position upon aggregation. A similar effect is seen for the aromatic protons at the inner position at the thiophene rings (H52, H57, H91). In contrast, thiophene protons at the outer position in close proximity to the NDI core (H50, H59, H84) experience deshielding to a range between 7.8 and 8 ppm, which can be attributed to the more planarized conformation in the stack. This deshielding of protons is consistent with the appearance of new chemical shifts in this region of the experimental spectra in bad solvents. However, complete assignment of all additional peaks is out of the scope of this work. The proposed back-folding of the polymer chain in bad solvents will result in a variety of additional conformations which are not covered by this simple approach.

In conclusion, the appearance of a new chemical shift in the NMR spectra directly proves the aggregation of P(NDI2OD-T2) in solvents like CF and toluene. NMR-DFT calculations allowed the exact assignment of the chemical shifts to the aromatic protons of nonaggregated P(NDI2OD-T2) in heated DCB. Based on a partially DFT optimized oligomer stack, we could explain the appearance of new peaks in the experimental spectra by aggregation.

Absorption and Fluorescence Spectroscopy of P(NDI2OD-T2) in Solvent Mixtures. Having established that aggregation plays a key role in describing the photophysics of P(NDI2OD-T2), we now turn to providing a detailed analysis of the changes of the optical properties as aggregate formation proceeds in mixtures of CN (good solvent) and toluene (poor solvent). Figure 6a shows the evolution of the solution spectra at 0.1 g/L polymer concentration with increasing toluene fraction. Addition of toluene gradually affects both the high-energy $\pi-\pi^*$ and the CT transitions. For the $\pi-\pi^*$ UV band, we observe mainly a change to longer wavelengths. Subtracting the absorption of the nonaggregated chains in CN shows that this spectral change is not a gradual solvatochromatic shift of a single peak, but rather is caused by the appearance and growth of a new absorption feature with the maximum at 405 nm. In contrast, the evolution of the long-wavelength absorption with increasing toluene content proceeds via two steps: first the appearance of a strong absorption at 710 nm (peak 1), and later the emergence of a shoulder at 815 nm (peak 2).

Figure 6b shows the PL of P(NDI2OD-T2) at 0.1 g/L in mixed CN:toluene solutions for increasing contents of toluene. These spectra have been recorded for excitation at 560 nm (which predominantly excites the nonaggregated chromophores) and at 420 nm (which predominantly excites

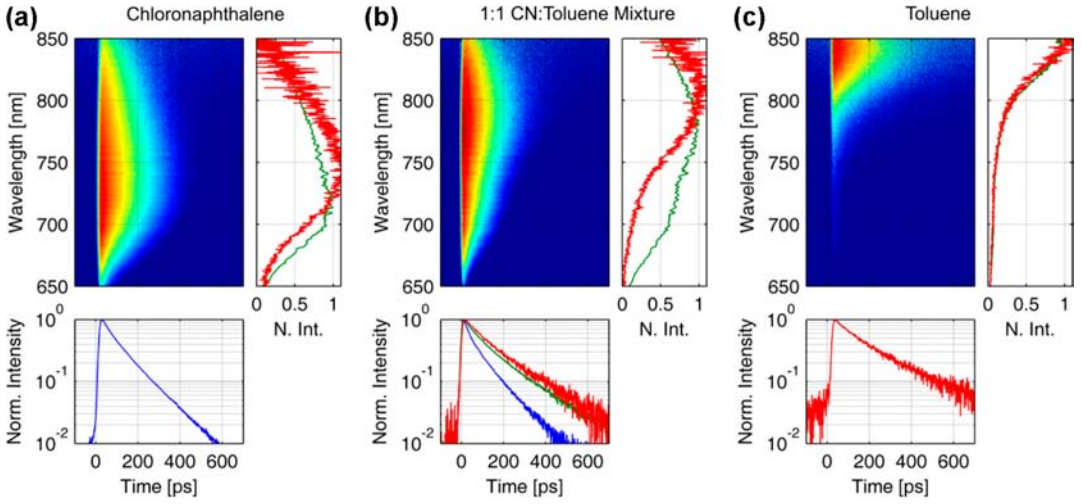

Figure 7. Streak camera images showing the PL after 390 nm excitation of 0.1 g/L solutions of (a) CN, (b) a 1:1 CN:toluene solvent mixture, and (c) toluene (logarithmic colormap). Normalized spectra are shown for early (0−50 ps, green line) and late (500−600 ps, red line) times. Normalized kinetics are shown for the intrachain exciton (710−730 nm, blue line), aggregate I (770−790 nm green line), and aggregate II (840−860 nm, red line).

aggregates). In both cases, the emission spectra at intermediate toluene content (∼40−70%) display a peak at 790 nm with a weak vibrational replica at ∼900 nm. As the toluene fraction increases, these spectral features become weaker and finally disappear at the highest toluene contents, when the aggregate PL becomes almost entirely dominated by emission peaks at 860 and 950 nm. These features, assigned to aggregate emission, are far more pronounced for excitation at 420 nm (Figure 6b bottom), which supports our previous interpretation of the absorption of nonaggregated and aggregated chains.

We emphasize that the evolution of the absorption of P(NDI2OD-T2) with decreasing solvent quality is distinctly different from the recently reported behavior of P3HT.[65] For P3HT, adding poor solvent leads to the appearance of a red-shifted absorption band with a well-resolved vibronic progression, assigned to aggregated chains. Increasing the concentration of poor solvent increases the overall strength of the low-energy band and alters the ratio of the 0−0 to the 0−1 vibrational peak, but it does not cause new absorption features to appear. For P(NDI2OD-T2), the distinct evolution of the absorption and emission spectra with increasing the toluene content suggests that chain collapse leads to two different aggregate species. In a first approximation, we term the species dominating the optical properties (with the main absorption at 710 nm and emission at 790 nm) at intermediate toluene content "aggregate I". The distinct emission features (and the 815 nm absorption feature) in pure toluene suggest that a second species exists that we will call "aggregate II". This species dominates the long-wavelength emission properties when the chain is in the highly aggregated state. The presence of two distinct emission spectra at different solvent mixing ratios rules out an alternative and simpler interpretation of the optical properties, where the long-wavelength absorption is due to one and the same aggregate species with the 0−0 and 0−1 vibronic bands at 815 and 710 nm, respectively, but where the 0−0 absorption strength is largely reduced at low to medium toluene content. Suppressed 0−0 absorption was predicted by Spano in H-aggregates with strong exciton coupling.[125] Noticeably this model also predicts that a reduction in the 0−0 absorption (e.g., when going from toluene to higher CN contents) should lead to an increase in the 0−2 absorption, which is not seen here (Figure 6a, bottom).

Time-Resolved Spectroscopy. In order to give substantial evidence for the existence of two different aggregate species, time-resolved PL measurements were performed. The emission of the CN solution, the toluene solution, and the 1:1 solution mixture were analyzed to determine the lifetimes of the intrachain exciton and aggregate species.

Figure 7 shows the time evolution of the PL of P(NDI2OD-T2) in CN, toluene, and a 1:1 CN:toluene mixture. The PL decay of the intramolecular exciton state present when the chains are extended in the good solvent CN (Figure 7a) is essentially monoexponential, with some red-shifting with time likely due to a structural relaxation of the excited state, or diffusion of excited states to lower energy sites. The lifetime of the exciton is 100 ps, found from a monoexponential fit of the emission decay averaged between 710 and 730 nm (see Supporting Information). Figure 7b shows the emission kinetics in the intermediate solvent mixture, where aggregation starts to alter the absorption and PL spectra (Figure 6). The dramatic change in the emission spectrum with time (illustrated in the integrated spectra between 0 and 50 ps and between 500 and 600 ps, green and red lines, respectively) indicates that the initial excited-state population evolves with time. In the early time spectrum (green line) a clear shoulder is visible at 700 nm, originating from exciton emission. This shoulder disappears completely from the late time spectrum (red line), indicating that after 500 ps the exciton population is negligible compared to the aggregate concentration. By fitting the 710−730 and 770−790 nm kinetics simultaneously to a biexponential function with the time constants shared between the wavelength regions, the quenched lifetime of the intrachain exciton is found to be 32 ps, and the lifetime of aggregate I is found to be 156 ps (see Supporting Information for details). From the ratio of the decay rates of the unquenched exciton population in CN to the quenched exciton population in the CN:toluene mixture, it is determined that ∼70% of the excitons are quenched in the solvent blend, indicating that the aggregate states play a primary role in the photophysics of P(NDI2OD-T2). Comparison to Figure 6 shows that the emission of the

dx.doi.org/10.1021/ja306844f | J. Am. Chem. Soc. 2012, 134, 18303−18317

aggregate peak at 800 nm agrees well with the aggregate I peak in the steady-state PL spectra.

Figure 7c shows that the emission kinetics in pure toluene are significantly different from those observed in either of the other two solutions. The emission shows one dominant peak at 850 nm, close to the edge of the sensitivity of the measurement setup. This agrees well with the peak position of aggregate II suggested by the steady-state spectroscopy (Figure 6). Examining the very early time emission in toluene, we see residual emission between 650 and 750 nm, indicating the presence of intrachain excitons in the excited-state population at the earliest of times. However, this emission is completely quenched within the instrument response time of the system. Therefore, the quenching of initially generated excitons is even more efficient in the toluene solution than in the solvent blend. Fitting the emission between 830 and 850 nm to a biexponential function with a component constrained to have a lifetime of the instrument response (15 ps) in order to account for the exciton emission reveals a lifetime for the aggregate II state of 170 ps, only slightly longer than that observed for aggregate I.

The presence of two distinct aggregate species becomes immediately clear by comparing the emission characteristics in the three solutions. The central figure of the emission in the solvent mixture cannot be expressed as a weighted sum of the species present in the two pure solvents. This gives clear evidence that an intermediate aggregate state (aggregate I) forms between the exciton on the extended chains and the aggregate II formed on the collapsed chains. We speculate that aggregate I might correspond to a dimer of like units stacked one on another, while aggregate II might correspond to the excitation delocalized over more than two like units in a larger stack. The two spectral signatures can also be caused by two distinct packing motifs with different degrees of overlap of the functional units. Therefore, the time-resolved emission spectroscopy confirms the existence of two forms of aggregate species and demonstrates the existence of efficient energy transfer from the exciton to the aggregate states.

The complete absence of emission features of aggregate I in the transient emission of P(NDI2OD-T2) in pure toluene taken immediately after excitation further suggests that this species has been completely replaced by aggregate II. This implies that the 710 nm peak in the absorption of P(NDI2OD-T2) in pure toluene is part of the vibronic progression of aggregate II absorption, and it does not originate from coexisting type I aggregates. In fact, adding ethyl acetate (EA), a very poor solvent for the polymer, to the toluene solution has only a minor effect on the shape of the long-wavelength absorption (for EA content up to 30%). The coincidence with respect to energy of the 0−1 transition of aggregate II with the lowest energy transition of aggregate I might be coincidental or caused by structural similarities of the two aggregates. Importantly, the deconvoluted absorption and emission spectra for different solvent mixing ratios, assuming that the solution in pure toluene comprises only nonaggregated chains and aggregate II, yielded consistent results (see Figure S6 and the corresponding discussion in the Supporting Information). Here, the contributions from aggregates I and II emerge at ∼20% and 40% toluene content, respectively, and the aggregate I contribution to both absorption and emission is maximum at a toluene concentration of ∼60%. Interestingly, the sum of the aggregate contributions in absorption and emission increases continuously and linearly with toluene content, without a visible change in the slope, suggesting that aggregate II is formed by replacing the intermediate aggregate I.

Analytical Ultracentrifugation. The spectroscopic investigations performed in the previous section undoubtedly reveal that aggregation of P(NDI2OD-T2) significantly changes the photophysical characteristics. We now illustrate the evolution of the microscopic structure that accompanies the changes of the optical properties. One remarkable result of the studies described above is that changing the polymer concentration has very little effect on the shape of the optical spectra, which is not reasonable if aggregation is an interchain process (Figure 2b). We therefore propose that aggregation of conjugated segments in solution occurs via stacking within polymer coils that contain one or very few polymer chains. This process might be initiated by a reduced swelling of the polymer coils in poor solvents. One well-established technique to analyze chain aggregation in solution is analytical ultracentrifugation (AUC). This method is well established in the field of biochemistry, but it is also widely used in modern colloidal analytics.[126,127]

In an AUC experiment, a spherical polymer coil of radius R, molecular mass M, and partial specific volume $\bar{v}$ sediments in the centrifugal field with a velocity given by the sedimentation coefficient s:[128,129]

$$s = \frac{M/N_A(1 - \bar{v}\rho)}{f} = \frac{M/N_A(1 - \bar{v}\rho)}{6\pi\eta R} \quad (1)$$

In eq 1, the frictional coefficient f is expressed by Stokes's law, N_A is the Avogadro constant, η is the viscosity and ρ the density of the solvent.

The determination of $\bar{v}$ (the inverse of the dry density ρ_P) of P(NDI2OD-T2) involved a typical density-variation AUC experiment[130] on the polymer in pure toluene and in a 1:1 mixture of deuterated toluene-d_8 and normal toluene. From our experiments (described in detail in the Supporting Information), we determined the dry density ρ_P of P(NDI2OD-T2) to be 1.1 g/cm^3. This value agrees very well with the density of P(NDI2OD-T2) crystallites according to X-ray diffraction data published by Rivnay et al. reporting a $\pi-\pi$ stacking distance of 3.93 Å, a lamella spacing of 25.5 Å, and the length of one repeat unit of 13.9 Å.[21] Assuming that this volume is occupied by one monomer (991.5 g/mol), we estimate the density of the ordered domains to be ρ_P = 1.18 g/cm^3. Since amorphous regions of P(NDI2OD-T2) will exhibit less density, this approach might overestimate the polymer dry density, well explaining the slightly smaller value of ρ_P = 1.1 g/cm^3 found by AUC here.

In the next step, the mass-average weights M_w of the P(NDI2OD-T2) particles (or agglomerates) in pure toluene and in mixtures with CN were measured by analyzing the equilibrium sedimentation profiles.[131,132] If an AUC experiment is conducted at moderate angular velocity, allowing back-diffusion of particles from the cell bottom, equilibrium between sedimentation and back-diffusion will be attained after a sufficient time. Evaluation of the stationary concentration profile yields an average molar mass M_w that is independent of the molecule size, shape, and swelling (see SI for details on the analysis).

Mean values for M_w deduced from these profiles are shown in Figure 8 for P(NDI2OD-T2) with M_w = 181 kDa (as determined by GPC) and a toluene content between 60% and 100%. Higher contents of CN lead to very slow sedimentation due to the small density contrast between CN and P(NDI2OD-

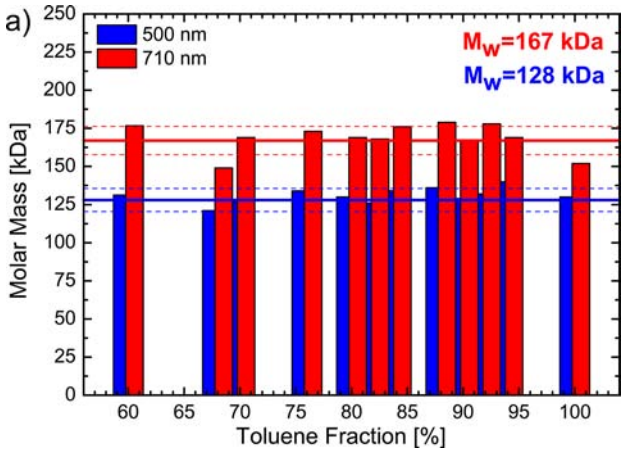

Figure 8. Molar mass of P(NDI2OD-T2) particles for a series of CN:toluene solvent mixtures determined by AUC equilibrium experiments at 500 and 710 nm and a polymer concentration between 0.04 and 0.1 g/L (depending on the solvent mixing ratio). Solid straight lines show the averaged M_w, while dashed lines indicate the standard deviation.

T2), drastically prolonging the time needed to reach equilibrium. The densities and viscosities of all solvent mixtures have been measured independently, as described in the Experimental Section.

Within the range of statistical deviation, the series clearly displays that the molar mass of the sedimenting particles is independent of the solvent mixture. There is no evidence for a systematic increase in particle (agglomerate) mass when increasing the toluene fraction from 60% to 100%. We note that equilibrium profiles measured at 500 nm yield a systematically smaller value of $M_w \approx 128$ kDa compared to 167 kDa at 710 nm. We understand this result as an indication of a lower degree of intrachain aggregation for shorter polymer chains, also visible in the M_w-dependent absorption spectra. Shorter chains are less likely aggregated than longer chains (see Figure 2b) and therefore are prevalently probed at 500 nm, where disordered P(NDI2OD-T2) absorbs. We underline that this difference is not a sign of agglomerate formation, since the fraction of toluene has no influence on the particle weight between 60% and 100%, where most of the changes in the optical spectra occur. We also measured equilibrium profiles on diluted P(NDI2OD-T2) solutions down to 0.01 g/L showing a very weak dependence on the determined M_w (Figure S10). This is a clear sign of weak interaction between the particles at a given concentration, thus supporting our interpretation from optical experiments that aggregation of P(NDI2OD-T2) in poor solvents is an intrachain process. Since lower toluene fractions could not be measured, we cannot rule out that addition of small amounts of toluene induces the formation of agglomerates comprising a small number of polymer chains, meaning that M_w determined from our AUC equilibrium runs is larger than the molar mass of a single chain. However, GPC measurements for this polymer batch reveal an average M_w = 181 kDa, very close to the value we determine here.

Sedimentation Velocity Experiments. At an angular velocity of 40 000 rpm, the polymer chains sediment fairly rapidly over a time frame of several hours. During this time, sedimentation profiles are taken every few minutes, yielding a data set of time-resolved and locally resolved absorption measurements. From various options for evaluation, we chose a model-independent, finite element fit on all scans as incorporated in SEDFIT,[133] yielding the sedimentation coefficient distribution $g(s)$, defined as the abundance of the species with the sedimentation coefficient s. Figure 9a shows an overlay of $g(s)$ distributions obtained from P(NDI2OD-T2) sedimentation velocity experiments of mixtures with 50% to 100% toluene content. Again it is obvious that sedimentation occurs more slowly with increasing CN content due to increasing viscosity and a smaller difference in density between solvent and solute. The distribution of the sedimentation coefficient $g(s)$ is rather broad for all solvent mixtures studied here, displaying the widespread molecular weights of our polymer batch.

If swelling of the particles occurs, the increased radius will directly lead to an enhanced friction. It is convenient to introduce the frictional ratio f/f_0, which relates the friction of the swollen polymer coil or agglomerate to the friction coefficient f_0 of a theoretical compact sphere of same mass and partial specific volume $\bar{\nu}$.[134] Since the maximum of the measured $g(s)$ distribution does not represent the average molecular weight, we used the averaged s of the $g(s)$ distribution for further analysis. We then directly calculated f/f_0 according to equation S3 as the quotient of the theoretical sedimentation coefficient of the compact sphere using the M_w derived from sedimentation equilibrium and the measured sedimentation coefficient average.

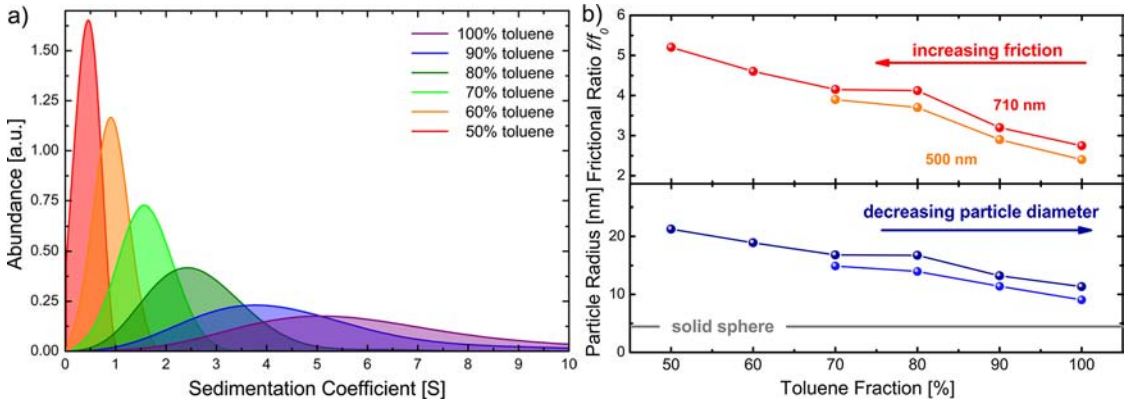

Figure 9. (a) Sedimentation coefficient distributions $g(s)$ of P(NDI2OD-T2) in a series of toluene:CN mixtures measured at an angular velocity of 40 000 rpm at 710 nm. (b) The upper graph shows the resulting frictional ratio f/f_0 in mixed solvent solutions, and the lower graph shows the particle radius probed at 500 and 710 nm.

dx.doi.org/10.1021/ja306844f | J. Am. Chem. Soc. 2012, 134, 18303−18317

Figure 9b plots the frictional ratio and the average radius R of the polymer coils/aggregates calculated according to eq 1. The results clearly show that the coils swell with increasing solubility from 10 nm radius in pure toluene to more than 20 nm in a 50% mixture of toluene with CN. Note that the radius in pure toluene is still ~3 times the radius R_0 predicted for a solid sphere. It can be also seen that data taken at 500 and 710 nm, probing different P(NDI2OD-T2) M_w fractions as explained previously, yield comparable results for the frictional ratio and coil diameter.

In summary, our sedimentation experiments provide solid support for our conclusions from optical experiments that aggregation of P(NDI2OD-T2) in solution proceeds within either individual polymer coils or preformed polymer aggregates, associated with a considerable decrease in the average diameter of the swollen polymer chain (or agglomerate) as schematically shown in Figure 10.

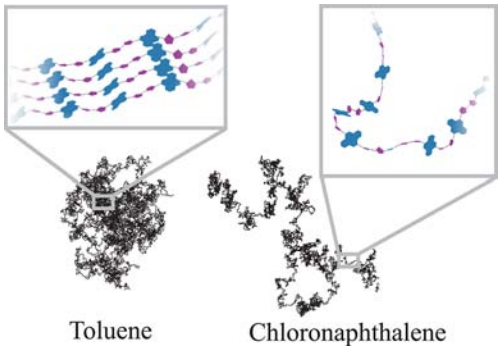

Figure 10. Schematic representation of the aggregation mechanism of P(NDI2OD-T2) in solution.

Aggregate Content and Film-Forming Process. Finally, we use the insight gained from the detailed investigation of P(NDI2OD-T2) structure in solution to understand the optical properties of thin films. Figure 11 shows absorption spectra of ~310 nm thick films of P(NDI2OD-T2) cast from solvents with different boiling points. It has been frequently reported that the morphology of thin conjugated polymer films can be altered by using solvents with higher boiling points, allowing the chains more time to rearrange while drying, but also by preaggregation in the pristine solution.[44,135] For example, Clark et al. analyzed the degree and quality of polymer crystallinity in layers of P3HT coated from solutions with the solvent boiling point ranging from 70 (CF) to 225 °C (TCB).[43] In this study, increasing boiling point caused a continuous rise of layer crystallinity from ~39% to 46%. These changes were clearly reflected in the vibronic progression of the polymer absorption, with a stronger 0−0 transition being related to improved intra- and interchain order. To our great surprise, P(NDI2OD-T2) films cast from toluene and trichlorobenzene, with drying times from seconds to minutes, deliver nearly identical absorption spectra (see Figure 11a). We propose that the transition from polymer chains in solution to solid P(NDI2OD-T2) involves chain aggregation within individual coils (or agglomerates), which progressively shrink upon decreasing the amount of solvent molecules in the drying layer. On the other hand, rearrangement of polymer chains in the final stage of drying seems to be rather insignificant. We point out that the peak positions attributed to aggregate absorption in the film are slightly blue-shifted compared to the solvent spectra, which we attribute to a different local environment.

By assigning the absorption of P(NDI2OD-T2) in CN to nonaggregated chains, we are now able to deconvolute the spectrum into contributions from amorphous and aggregated areas. Quantification of the layers' aggregate content from a deconvolution of the thin-film absorption requires knowledge of the oscillator strength of chains in the aggregated state relative to that of chains in the amorphous state, $\varepsilon_{aggr}/\varepsilon_{amorph}$. Clark et al. employed temperature-dependent absorbance studies on P3HT, which yielded $\varepsilon_{aggr}/\varepsilon_{amorph} \approx 1.3$.[43] A similar value was determined by Scharsich et al. by relating absorption spectra of high-molecular-weight P3HT in pure toluene (which is a good solvent for the polymer) and in mixtures of toluene with EA.[65] For P(NDI2OD-T2), analysis of the data plotted in Figure S6c for different toluene:CN mixing ratios yields $\varepsilon_{aggr}/\varepsilon_{amorph} \approx 2.5$. Note that this analysis does not differentiate between aggregates I and II, as the sum of the corresponding absorption bands in Figure S6c increases continuously with increasing toluene fraction.

For further analysis, the amorphous contribution was subtracted from each film spectrum, and the residue was integrated between 500 and 900 nm and divided by the integrated amorphous contribution. Multiplication by $(\varepsilon_{aggr}/\varepsilon_{amorph})^{-1}$ then yielded the layer aggregate content. This procedure revealed that ~45% of the chains in the as-prepared

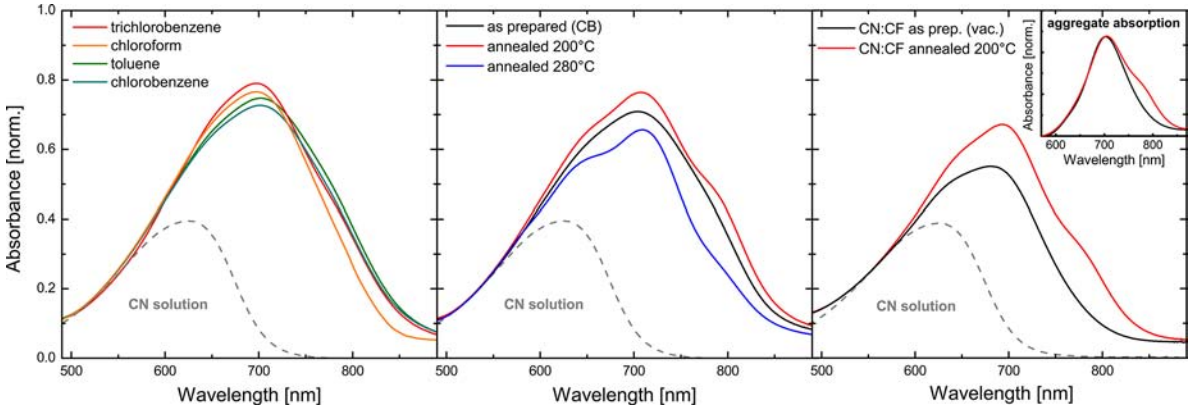

Figure 11. Room-temperature absorption of P(NDI2OD-T2) films (310 nm) cast from different solvents (a), layers coated from chlorobenzene and annealed at different temperatures (b), and films prepared from CN:CF mixtures and subsequent vacuum drying (c) (see text). For comparison, the solution spectrum in CN is shown.

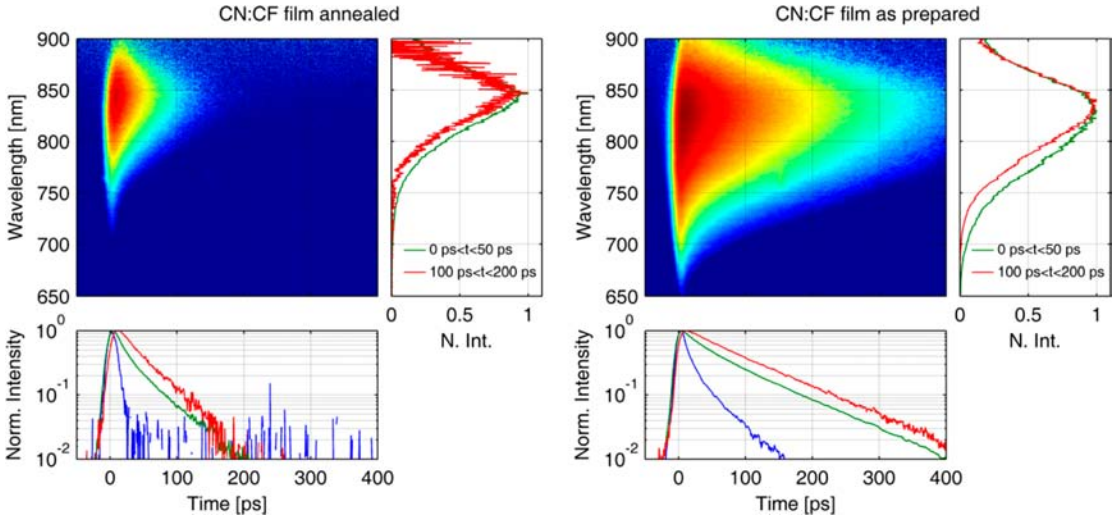

Figure 12. Streak camera images showing the PL after 390 nm excitation of annealed (left) and as-prepared films (right) cast from a CN:CF mixture (logarithmic colormap). Normalized spectra are shown for early (0−50 ps, green line) and late (100−200 ps, red line) times. Normalized kinetics are shown for the intrachain exciton (690−700 nm, blue line), aggregate I (770−800 nm green line), and aggregate II (850−900 nm, red line).

layers are in the aggregated state, rather independent of preparation. Although no distinct vibronic structure is evident, as-cast films of P(NDI2OD-T2) contain a significant amount of aggregates.

Figure 11b also shows the spectra of films coated from chlorobenzene followed by annealing at different temperatures. Upon annealing of the films at temperatures below 200 °C, the aggregate contribution increases only slightly, accompanied with a narrowing of the vibronic progression line width. Obviously, annealing is not an effective way to further increase the amount of aggregates formed in the films after preparation. The observed line width narrowing can be explained by minor chain reorganization within the aggregate itself. Annealing above 200 °C leads to a decrease in aggregate content. It has been shown previously that annealing the films up to the melting temperature (~310 °C)[11] in inert atmosphere does not induce any decomposition or degradation of the material.[22] However, due to the large polydispersity of this material, the melting point is not well defined, and low-molecular-weight fractions will melt at lower temperatures. We therefore propose that premelting below T_m leads to the reduction in aggregate content.[136]

It has been proposed previously that annealing P(NDI2OD-T2) films above the melting point followed by rapid temperature quenching leads to amorphous films.[22] We applied this approach to films coated from chlorobenzene and found the absorbance of such films to be quite similar to spectra of quenched films presented previously.[22] Nevertheless, these films still demonstrate clear aggregate features and cannot be considered as completely amorphous. This might be one reason why these films still showed considerable electron field-effect mobilities.

We found that films with very weak aggregate II absorption can be prepared as follows. First, a film was coated from a solvent mixture containing the good solvent CN in combination with the fast-drying solvent CF. Films coated from the high-boiling-point solvent CN dried very slowly and suffered from dewetting. However, mixing with the fast-drying component CF "fixes" the wet film after spin-coating. These wet films were then quickly transferred to vacuum in order to evaporate the remaining CN. This procedure is similar to the preparation routine we suggested for the preparation of P3HT:P(NDI2OD-T2) solar cells,[30] modified to include vacuum drying. The resulting absorption of such prepared and annealed films is shown in Figure 11c. Comparison with the solution spectra suggests that the as-prepared CN:CF films mainly consist of aggregate I. Annealing at 200 °C leads to an increase of the 785 nm peak, indicative of the growth of aggregate II in the thin film.

To address the transient photophysical properties of these films, we have performed time-resolved emission and transient absorption spectroscopy. In Figure 12 we show that the film after annealing has emission properties similar to those of the pure toluene solution, shown in Figure 7c. From this we conclude that all excitons on single chains are quickly quenched by transfer to aggregate II species. We note, however, that the lifetime of aggregate II is significantly shorter in the annealed film (44 ps compared to 170 ps) than in solution. Faster nonradiative recombination, likely caused by transfer to quenching sites, would explain this decrease. In the as-cast film the emission kinetics appear to result from a combination of the aggregate I and aggregate II species, as observed in the CN:toluene mixture and pure toluene solutions, respectively. The emission of the aggregate II species is longer than in the annealed film, more similar to that observed in solution although still somewhat shorter. This is consistent with the aggregate II sites being more widely spaced before the film is annealed, meaning excitons cannot move easily between aggregated domains, and therefore their encounter with quenching sites may play a smaller role in reducing their lifetime. The transient PL data suggest that as-prepared CN:CF films mainly consist of aggregate I, while annealing leads to a transition to aggregate II. This statement is further substantiated by the results from ultrafast transient absorption spectroscopy presented in Figure S12.

■ SUMMARY

In conclusion, we have shown distinct changes in the optical absorption and emission spectra of P(NDI2OD-T2) in solution when varying the organic solvent or the solvent mixture ratio. Detailed analyses of these changes in combination with NMR and AUC studies suggest that P(NDI2OD-T2) form aggregates

in almost all organic solvents, even at low concentrations, which we attribute to the aggregation of chain segments with single chains or agglomerates containing only few chains. The optical characteristics of nonaggregate chains, with an absorption maximum at 520 nm and an emission maximum at 715 nm, are observed only when using solvent molecules with extended and highly polarizable aromatic cores such as CN. This assignment is fully supported by DFT calculation on isolated chains. In contrast, the optical spectra of P(NDI2OD-T2) in common solvents like CF, toluene, etc. are dominated by aggregates with distinct long-wavelength absorption and emission features. Our DFT calculations on optimized stack structures revealed chain planarization as the main cause for the observed red-shifts. A more detailed analysis of the steady-state and transient optical spectra in mixtures of CN and toluene suggests that aggregation of P(NDI2OD-T2) occurs via an intermediate state (aggregate I), and that this intermediate is fully replaced by a second species (aggregate II) with lower absorption and emission energies when going to pure toluene.

Since P(NDI2OD-T2) forms aggregates in most organic solvents, we expected that layers prepared by spin-coating from these solvents would consist of an assembly of collapsed coils with high local order. Flattening of the globuli during spin-coating and drying might explain the unconventional face-on orientation of the NDI cores as observed by GIXD.[21] Deconvolution of the absorption spectra allowed us to determine the aggregate content in as-prepared spin-coated layers to be ∼45%. This value compares well to the degree of crystallinity in as-prepared pristine P3HT layers reported by Clark et al.[43] Steady-state and transient optical spectroscopy reveals the characteristic features of aggregates II. Schuettfort et al. used X-ray scattering to estimate the size of a crystalline domain in films of P(NDI2OD-T2) with $M_w \approx 100\,000$ g/mol.[22] Their measurement on as-prepared samples coated from DCB yielded an approximate crystalline domain size of 10.4 nm in both the lamellar and the backbone directions. As the volume of a single collapsed chain with the given molecular weight and a dry density of 1.1 g/cm^3 is ∼150 nm^3, we propose that these aggregates consist of a rather small number of collapsed chains.

Interestingly, the optical properties of our films are independent of the solvent used for spin-coating. This indicates that rapid chain collapse dominates film formation even when coating from a good solvent like CN. This process also inhibits the formation of amorphous and disordered P(NDI2OD-T2) films. Suppression of aggregate II formation was only achieved when the film was spin-coated from a solvent mixture of CN in combination with the fast-drying solvent CF, followed by rapid drying in vacuum. The optical properties of these layers were dominated by aggregate I.

Annealing of regularly coated films had little influence on the optical spectra and the degree of aggregation. Schuettfort et al. reported the crystallite size in the (100) and (001) direction to increase significantly upon annealing.[22] Also, Rivnay et al. noted a considerable increase of the (100) peak intensity upon annealing up to 250 °C, accompanied by a slight decrease in line width.[23] Apparently, annealing improves interchain order on the length scale of several tens of nanometers, most likely by merging smaller crystallites, while it barely changes the local degree of order as addressed by optical spectroscopy.

Finally, we note that scanning transmission X-ray microscopy studies by Sciascia and co-workers on P(NDI2OD-T2) films annealed at 110 °C revealed common preferential alignment of polymer backbones within domains of 0.5−1 μm in length, but with a rather low degree of orientational order (∼17%).[24] Domains of similar size were previously seen in atomic force microscopy phase contrast and polarized microscopy images of as-prepared and annealed P(NDI2OD-T2) films.[23] The resolution of these techniques, however, is not sufficient to image order on the length scale of aggregates comprising only a few collapsed chains. We propose that these large domains consist of small crystallites, as determined by GIXD,[22,23] with partially correlated orientation on the micrometer length scale. Despite the rather poor degree of order on the larger scale, these layers exhibit very high in- and out-of-plane mobilities, even when carriers need to travel several micrometers in distance. Our optical spectroscopy data reveal that almost 50% of the chains are indeed in the aggregate state, and that this fraction changes only a little upon thermal treatment. Following common interpretations to explain the dependence of mobility on molecular weight in P3HT,[4,9,65,136,137] we propose that these aggregates are bridged via long tie chains, which allow charges to avoid being trapped at grain boundaries and to move rapidly between aggregates. This interconnection of stable chain aggregates might also be responsible for the small effect annealing has on the carrier mobility in thin P(NDI2OD-T2).[22,23]

■ ASSOCIATED CONTENT

Supporting Information

Experimental details, table of solvent properties, excitation spectra in toluene and CN, QC calculations in different solvents, NMR atom numbering and P(NDI2OD-T2) trimer stacking structure, detailed decomposition of the CN:toluene solvent series spectra, analysis of the transient data in solution, description and analysis of the AUC density variation and equilibrium experiments and transient absorption data on CN:CF films. This material is available free of charge via the Internet at http://pubs.acs.org.

■ AUTHOR INFORMATION

Corresponding Author

neher@uni-potsdam.de

Notes

The authors declare no competing financial interest.

■ ACKNOWLEDGMENTS

Kai Saalwächter (University Halle) is gratefully acknowledged for fruitful discussions regarding the NMR analysis. The authors thank Andreas Hünermund (University Potsdam), Tina Franke, and Doreen Freund (Nanolytics GmbH) for laboratory assistance. The work in Potsdam was financially supported by the German Federal Ministry of Science and Education (BMBF FKZ 03X3525D) and the German Research Foundation (DFG SPP 1355).

■ REFERENCES

(1) Beaujuge, P. M.; Frechet, J. M. J. *J. Am. Chem. Soc.* **2011**, *133*, 20009.

(2) Sirringhaus, H.; Brown, P. J.; Friend, R. H.; Nielsen, M. M.; Bechgaard, K.; Langeveld-Voss, B. M. W.; Spiering, A. J. H.; Janssen, R. A. J.; Meijer, E. W.; Herwig, P.; de Leeuw, D. M. *Nature* **1999**, *401*, 685.

(3) Donley, C. L.; Zaumseil, J.; Andreasen, J. W.; Nielsen, M. M.; Sirringhaus, H.; Friend, R. H.; Kim, J. S. *J. Am. Chem. Soc.* **2005**, *127*, 12890.

(4) Kline, R. J.; McGehee, M. D.; Kadnikova, E. N.; Liu, J. S.; Frechet, J. M. J.; Toney, M. F. *Macromolecules* **2005**, *38*, 3312.
(5) Kline, R. J.; McGehee, M. D.; Kadnikova, E. N.; Liu, J. S.; Frechet, J. M. J. *Adv. Mater.* **2003**, *15*, 1519.
(6) Salleo, A. *Mater. Today* **2007**, *10*, 38.
(7) Jimison, L. H.; Toney, M. F.; McCulloch, I.; Heeney, M.; Salleo, A. *Adv. Mater.* **2009**, *21*, 1568.
(8) Zen, A.; Pflaum, J.; Hirschmann, S.; Zhuang, W.; Jaiser, F.; Asawapirom, U.; Rabe, J. P.; Scherf, U.; Neher, D. *Adv. Funct. Mater.* **2004**, *14*, 757.
(9) Zen, A.; Saphiannikova, M.; Neher, D.; Grenzer, J.; Grigorian, S.; Pietsch, U.; Asawapirom, U.; Janietz, S.; Scherf, U.; Lieberwirth, I.; Wegner, G. *Macromolecules* **2006**, *39*, 2162.
(10) Rivnay, J.; Noriega, R.; Northrup, J. E.; Kline, R. J.; Toney, M. F.; Salleo, A. *Phys. Rev. B* **2011**, *83*, 4.
(11) Yan, H.; Chen, Z. H.; Zheng, Y.; Newman, C.; Quinn, J. R.; Dotz, F.; Kastler, M.; Facchetti, A. *Nature* **2009**, *457*, 679.
(12) Steyrleuthner, R.; Schubert, M.; Jaiser, F.; Blakesley, J. C.; Chen, Z.; Facchetti, A.; Neher, D. *Adv. Mater.* **2010**, *22*, 2799.
(13) Caironi, M.; Newman, C.; Moore, J. R.; Natali, D.; Yan, H.; Facchetti, A.; Sirringhaus, H. *Appl. Phys. Lett.* **2010**, *96*, 3.
(14) Rao, M.; Ponce Ortiz, R.; Facchetti, A.; Marks, T. J.; Narayan, K. S. *J. Phys. Chem. C* **2010**, *114*, 20609.
(15) Blakesley, J. C.; Schubert, M.; Steyrleuthner, R.; Chen, Z. H.; Facchetti, A.; Neher, D. *Appl. Phys. Lett.* **2011**, *99*, 3.
(16) Li, J. H.; Du, J.; Xu, J. B.; Chan, H. L. W.; Yan, F. *Appl. Phys. Lett.* **2012**, *100*, 4.
(17) Baeg, K.-J.; Khim, D.; Jung, S.-W.; Kang, M.; You, I.-K.; Kim, D.-Y.; Facchetti, A.; Noh, Y.-Y. *Adv. Mater.* **2012**, DOI: 10.1002/adma.201201464.
(18) Lange, I.; Blakesley, J. C.; Frisch, J.; Vollmer, A.; Koch, N.; Neher, D. *Phys. Rev. Lett.* **2011**, *106*, 4.
(19) Caironi, M.; Bird, M.; Fazzi, D.; Chen, Z.; Di Pietro, R.; Newman, C.; Facchetti, A.; Sirringhaus, H. *Adv. Funct. Mater.* **2011**, *21*, 3371.
(20) Fazzi, D.; Caironi, M.; Castiglioni, C. *J. Am. Chem. Soc.* **2011**, *133*, 19056.
(21) Rivnay, J.; Toney, M. F.; Zheng, Y.; Kauvar, I. V.; Chen, Z.; Wagner, V.; Facchetti, A.; Salleo, A. *Adv. Mater.* **2010**, *22*, 4359.
(22) Schuettfort, T.; Huettner, S.; Lilliu, S.; Macdonald, J. E.; Thomsen, L.; McNeill, C. R. *Macromolecules* **2011**, *44*, 1530.
(23) Rivnay, J.; Steyrleuthner, R.; Jimison, L. H.; Casadei, A.; Chen, Z.; Toney, M. F.; Facchetti, A.; Neher, D.; Salleo, A. *Macromolecules* **2011**, *44*, 5246.
(24) Sciascia, C.; Martino, N.; Schuettfort, T.; Watts, B.; Grancini, G.; Antognazza, M. R.; Zavelani-Rossi, M.; McNeill, C. R.; Caironi, M. *Adv. Mater.* **2011**, *23*, 5086.
(25) Fabiano, S.; Chen, Z.; Vahedi, S.; Facchetti, A.; Pignataro, B.; Loi, M. A. *J. Mater. Chem.* **2011**, *21*, 5891.
(26) Moore, J. R.; Albert-Seifried, S.; Rao, A.; Massip, S.; Watts, B.; Morgan, D. J.; Friend, R. H.; McNeill, C. R.; Sirringhaus, H. *Adv. Energy Mater.* **2011**, *1*, 230.
(27) Kim, J. B.; Lee, S.; Toney, M. F.; Chen, Z.; Facchetti, A.; Kim, Y. S.; Loo, Y.-L. *Chem. Mater.* **2010**, *22*, 4931.
(28) Holcombe, T. W.; Norton, J. E.; Rivnay, J.; Woo, C. H.; Goris, L.; Piliego, C.; Griffini, G.; Sellinger, A.; Bredas, J. L.; Salleo, A.; Frechet, J. M. J. *J. Am. Chem. Soc.* **2011**, *133*, 12106.
(29) Yan, H.; Collins, B. A.; Gann, E.; Wang, C.; Ade, H.; McNeill, C. R. *ACS Nano* **2012**, *6*, 677.
(30) Schubert, M.; Dolfen, D.; Frisch, J.; Roland, S.; Steyrleuthner, R.; Stiller, B.; Chen, Z.; Scherf, U.; Koch, N.; Facchetti, A.; Neher, D. *Adv. Energy Mater.* **2012**, *2*, 369.
(31) Graser, F.; Hadicke, E. *Liebigs Ann. Chem.* **1980**, 1994.
(32) Graser, F.; Hadicke, E. *Liebigs Ann. Chem.* **1984**, 483.
(33) Klebe, G.; Graser, F.; Hadicke, E.; Berndt, J. *Acta Crystallogr. Sect. B-Struct. Commun.* **1989**, *45*, 69.
(34) Kazmaier, P. M.; Hoffmann, R. *J. Am. Chem. Soc.* **1994**, *116*, 9684.
(35) Wurthner, F.; Thalacker, C.; Diele, S.; Tschierske, C. *Chem. Eur. J.* **2001**, *7*, 2245.
(36) Wurthner, F. *Chem. Commun.* **2004**, 1564.
(37) Chen, Z. J.; Stepanenko, V.; Dehm, V.; Prins, P.; Siebbeles, L. D. A.; Seibt, J.; Marquetand, P.; Engel, V.; Wurthner, F. *Chem. Eur. J.* **2007**, *13*, 436.
(38) Turner, S. T.; Pingel, P.; Steyrleuthner, R.; Crossland, E. J. W.; Ludwigs, S.; Neher, D. *Adv. Funct. Mater.* **2011**, *21*, 4640.
(39) Scharsich, C.; Lohwasser, R. H.; Sommer, M.; Asawapirom, U.; Scherf, U.; Thelakkat, M.; Neher, D.; Kohler, A. *J. Polym. Sci. Pt. B: Polym. Phys.* **2011**, *50*, 442.
(40) Brown, P. J.; Thomas, D. S.; Kohler, A.; Wilson, J. S.; Kim, J. S.; Ramsdale, C. M.; Sirringhaus, H.; Friend, R. H. *Phys. Rev. B* **2003**, *67*, 16.
(41) Clark, J.; Silva, C.; Friend, R. H.; Spano, F. C. *Phys. Rev. Lett.* **2007**, *98*, 4.
(42) Spano, F. C. *J. Chem. Phys.* **2005**, *122*, 15.
(43) Clark, J.; Chang, J. F.; Spano, F. C.; Friend, R. H.; Silva, C. *Appl. Phys. Lett.* **2009**, *94*, 3.
(44) Nguyen, T. Q.; Doan, V.; Schwartz, B. J. *J. Chem. Phys.* **1999**, *110*, 4068.
(45) Traiphol, R.; Potai, R.; Charoenthai, N.; Srikhirin, T.; Kerdcharoen, T.; Osotchan, T. *J. Polym. Sci. Pt. B: Polym. Phys.* **2010**, *48*, 894.
(46) Traiphol, R.; Sanguansat, P.; Srikhirin, T.; Kerdcharoen, T.; Osotchan, T. *Macromolecules* **2006**, *39*, 1165.
(47) Padmanaban, G.; Ramakrishnan, S. *J. Phys. Chem. B* **2004**, *108*, 14933.
(48) Nguyen, T. Q.; Martini, I. B.; Liu, J.; Schwartz, B. J. *J. Phys. Chem. B* **2000**, *104*, 237.
(49) Collison, C. J.; Rothberg, L. J.; Treemaneekarn, V.; Li, Y. *Macromolecules* **2001**, *34*, 2346.
(50) Schindler, F.; Lupton, J. M.; Feldmann, J.; Scherf, U. *Proc. Natl. Acad. Sci. U.S.A.* **2004**, *101*, 14695.
(51) Huser, T.; Yan, M. *J. Photochem. Photobiol. A-Chem.* **2001**, *144*, 43.
(52) Grell, M.; Bradley, D. D. C.; Ungar, G.; Hill, J.; Whitehead, K. S. *Macromolecules* **1999**, *32*, 5810.
(53) Grell, M.; Bradley, D. D. C.; Long, X.; Chamberlain, T.; Inbasekaran, M.; Woo, E. P.; Soliman, M. *Acta Polym.* **1998**, *49*, 439.
(54) Dias, F. B.; Morgado, J.; Macanita, A. L.; da Costa, F. P.; Burrows, H. D.; Monkman, A. P. *Macromolecules* **2006**, *39*, 5854.
(55) Peet, J.; Kim, J. Y.; Coates, N. E.; Ma, W. L.; Moses, D.; Heeger, A. J.; Bazan, G. C. *Nat. Mater.* **2007**, *6*, 497.
(56) Blouin, N.; Michaud, A.; Gendron, D.; Wakim, S.; Blair, E.; Neagu-Plesu, R.; Belletête, M.; Durocher, G.; Tao, Y.; Leclerc, M. *J. Am. Chem. Soc.* **2007**, *130*, 732.
(57) Hou, J.; Chen, H.-Y.; Zhang, S.; Li, G.; Yang, Y. *J. Am. Chem. Soc.* **2008**, *130*, 16144.
(58) Lee, J. K.; Ma, W. L.; Brabec, C. J.; Yuen, J.; Moon, J. S.; Kim, J. Y.; Lee, K.; Bazan, G. C.; Heeger, A. J. *J. Am. Chem. Soc.* **2008**, *130*, 3619.
(59) Wienk, M. M.; Turbiez, M.; Gilot, J.; Janssen, R. A. J. *Adv. Mater.* **2008**, *20*, 2556.
(60) Chen, H.-Y.; Hou, J.; Hayden, A. E.; Yang, H.; Houk, K. N.; Yang, Y. *Adv. Mater.* **2010**, *22*, 371.
(61) Gu, Y.; Wang, C.; Russell, T. P. *Adv. Energy Mater.* **2012**, *2*, 683.
(62) Jespersen, K. G.; Beenken, W. J. D.; Zaushitsyn, Y.; Yartsev, A.; Andersson, M.; Pullerits, T.; Sundstrom, V. *J. Chem. Phys.* **2004**, *121*, 12613.
(63) Nigam, S.; Rutan, S. *Appl. Spectrosc.* **2001**, *55*, 362A.
(64) Suppan, P. *J. Photochem. Photobiol. A: Chem.* **1990**, *50*, 293.
(65) Scharsich, C.; Lohwasser, R. H.; Sommer, M.; Asawapirom, U.; Scherf, U.; Thelakkat, M.; Neher, D.; Köhler, A. *J. Polym. Sci. Pt. B: Polym. Phys.* **2012**, *50*, 442.
(66) Köhler, A.; Hoffmann, S. T.; Bässler, H. *J. Am. Chem. Soc.* **2012**, *134*, 11594.
(67) Gierschner, J.; Cornil, J.; Egelhaaf, H. J. *Adv. Mater.* **2007**, *19*, 173.

(68) Risko, C.; McGehee, M. D.; Bredas, J.-L. *Chem. Sci.* **2011**, *2*, 1200.
(69) Van Vooren, A.; Kim, J. S.; Cornil, J. *Chemphyschem* **2008**, *9*, 989.
(70) Zhang, L.; Zhang, Q. Y.; Ren, H.; Yan, H. L.; Zhang, J. P.; Zhang, H. P.; Gu, J. W. *Sol. Energy Mater. Sol. Cells* **2008**, *92*, 581.
(71) Karsten, B. P.; Viani, L.; Gierschner, J.; Cornil, J.; Janssen, R. A. J. *J. Phys. Chem. A* **2009**, *113*, 10343.
(72) Milian Medina, B.; Van Vooren, A.; Brocorens, P.; Gierschner, J.; Shkunov, M.; Heeney, M.; McCulloch, I.; Lazzaroni, R.; Cornil, J. *Chem. Mater.* **2007**, *19*, 4949.
(73) Karsten, B. P.; Viani, L.; Gierschner, J.; Cornil, J.; Janssen, R. A. J. *J. Phys. Chem. A* **2008**, *112*, 10764.
(74) Salzner, U.; Lagowski, J. B.; Pickup, P. G.; Poirier, R. A. *J. Comput. Chem.* **1997**, *18*, 1943.
(75) Cornil, J.; Gueli, I.; Dkhissi, A.; Sancho-Garcia, J. C.; Hennebicq, E.; Calbert, J. P.; Lemaur, V.; Beljonne, D.; Bredas, J. L. *J. Chem. Phys.* **2003**, *118*, 6615.
(76) Salzner, U.; Karalti, O.; Durdagi, S. *J. Mol. Modell.* **2006**, *12*, 687.
(77) Scharber, M. C.; Koppe, M.; Gao, J.; Cordella, F.; Loi, M. A.; Denk, P.; Morana, M.; Egelhaaf, H. J.; Forberich, K.; Dennler, G.; Gaudiana, R.; Waller, D.; Zhu, Z. G.; Shi, X. B.; Brabec, C. J. *Adv. Mater.* **2010**, *22*, 367.
(78) Zhang, X.; Steckler, T. T.; Dasari, R. R.; Ohira, S.; Potscavage, W. J.; Tiwari, S. P.; Coppee, S.; Ellinger, S.; Barlow, S.; Bredas, J. L.; Kippelen, B.; Reynolds, J. R.; Marder, S. R. *J. Mater. Chem.* **2010**, *20*, 123.
(79) Blouin, N.; Michaud, A.; Gendron, D.; Wakim, S.; Blair, E.; Neagu-Plesu, R.; Belletete, M.; Durocher, G.; Tao, Y.; Leclerc, M. *J. Am. Chem. Soc.* **2008**, *130*, 732.
(80) Peng, Q.; Park, K.; Lin, T.; Durstock, M.; Dai, L. M. *J. Phys. Chem. B* **2008**, *112*, 2801.
(81) Mondal, R.; Ko, S.; Norton, J. E.; Miyaki, N.; Becerril, H. A.; Verploegen, E.; Toney, M. F.; Bredas, J. L.; McGehee, M. D.; Bao, Z. N. *J. Mater. Chem.* **2009**, *19*, 7195.
(82) Mondal, R.; Miyaki, N.; Becerril, H. A.; Norton, J. E.; Parmer, J.; Mayer, A. C.; Tang, M. L.; Bredas, J. L.; McGehee, M. D.; Bao, Z. A. *Chem. Mater.* **2009**, *21*, 3618.
(83) Steckler, T. T.; Zhang, X.; Hwang, J.; Honeyager, R.; Ohira, S.; Zhang, X. H.; Grant, A.; Ellinger, S.; Odom, S. A.; Sweat, D.; Tanner, D. B.; Rinzler, A. G.; Barlow, S.; Bredas, J. L.; Kippelen, B.; Marder, S. R.; Reynolds, J. R. *J. Am. Chem. Soc.* **2009**, *131*, 2824.
(84) Chen, H. Y.; Hou, J. H.; Hayden, A. E.; Yang, H.; Houk, K. N.; Yang, Y. *Adv. Mater.* **2010**, *22*, 371.
(85) Liu, B.; Najari, A.; Pan, C. Y.; Leclerc, M.; Xiao, D. Q.; Zou, Y. P. *Macromol. Rapid Commun.* **2010**, *31*, 391.
(86) Persson, N. K.; Sun, M. T.; Kjellberg, P.; Pullerits, T.; Inganas, O. *J. Chem. Phys.* **2005**, *123*, 9.
(87) Bredas, J. L.; Beljonne, D.; Coropceanu, V.; Cornil, J. *Chem. Rev.* **2004**, *104*, 4971.
(88) Winfield, J. M.; Van Vooren, A.; Park, M. J.; Hwang, D. H.; Cornil, J.; Kim, J. S.; Friend, R. H. *J. Chem. Phys.* **2009**, *131*, 5.
(89) Mondal, R.; Becerril, H. A.; Verploegen, E.; Kim, D.; Norton, J. E.; Ko, S.; Miyaki, N.; Lee, S.; Toney, M. F.; Bredas, J. L.; McGehee, M. D.; Bao, Z. N. *J. Mater. Chem.* **2010**, *20*, 5823.
(90) Becke, A. D. *J. Chem. Phys.* **1993**, *98*, 5648.
(91) Lee, C. T.; Yang, W. T.; Parr, R. G. *Phys. Rev. B* **1988**, *37*, 785.
(92) Schäfer, A.; Horn, H.; Ahlrichs, R. *J. Chem. Phys.* **1992**, *97*, 2571.
(93) Schäfer, A.; Huber, C.; Ahlrichs, R. *J. Chem. Phys.* **1994**, *100*, 5829.
(94) TURBOMOLE V6.3 2011, a development of University of Karlsruhe and Forschungszentrum Karlsruhe GmbH, 1989−2007, TURBOMOLE GmbH, since 2007; available from www.turbomole.com.
(95) Yanai, T.; Tew, D. P.; Handy, N. C. *Chem. Phys. Lett.* **2004**, *393*, 51.
(96) Frisch, M. J.; Trucks, G. W.; Schlegel, H. B.; Scuseria, G. E.; Robb, M. A.; Cheeseman, J. R.; Scalmani, G. B., V.; Mennucci, B.; Petersson, G. A.; Nakatsuji, H.; Caricato, M.; Li, X.; Hratchian, H. P.; Izmaylov, A. F.; Bloino, J.; Zheng, G.; Sonnenberg, J. L.; Hada, M.; Ehara, M.; Toyota, K.; Fukuda, R.; Hasegawa, J.; Ishida, M.; Nakajima, T.; Honda, Y.; Kitao, O.; Nakai, H.; Vreven, T.; Montgomery, J. A., Jr.; Peralta, J. E.; Ogliaro, F.; Bearpark, M.; Heyd, J. J.; Brothers, E.; Kudin, K. N.; Staroverov, V. N.; Kobayashi, R.; Normand, J.; Raghavachari, K.; Rendell, A.; Burant, J. C.; Iyengar, S. S.; Tomasi, J.; Cossi, M.; Rega, N.; Millam, J. M.; Klene, M.; Knox, J. E.; Cross, J. B.; Bakken, V.; Adamo, C.; Jaramillo, J.; Gomperts, R.; Stratmann, R. E.; Yazyev, O.; Austin, A. J.; Cammi, R.; Pomelli, C.; Ochterski, J. W.; Martin, R. L.; Morokuma, K.; Zakrzewski, V. G.; Voth, G. A.; Salvador, P.; Dannenberg, J. J.; Dapprich, S.; Daniels, A. D.; Farkas, Ö.; Foresman, J. B.; Ortiz, J. V.; Cioslowski, J.; Fox, D. J. *Gaussian 09*, Revision A.02; Gaussian, Inc.: Wallingford, CT, 2009.
(97) Peach, M. J. G.; Cohen, A. J.; Tozer, D. J. *Phys. Chem. Chem. Phys.* **2006**, *8*, 4543.
(98) Jacquemin, D.; Wathelet, V.; Perpete, E. A.; Adamo, C. *J. Chem. Theory Comput.* **2009**, *5*, 2420.
(99) Grimme, S. *J. Comput. Chem.* **2006**, *27*, 1787.
(100) Garreau, S.; Leclerc, M.; Errien, N.; Louarn, G. *Macromolecules* **2003**, *36*, 692.
(101) Yang, C.; Orfino, F. P.; Holdcroft, S. *Macromolecules* **1996**, *29*, 6510.
(102) Iwasaki, K.; Fujimoto, H.; Matsuzaki, S. *Synth. Met.* **1994**, *63*, 101.
(103) Inganas, O.; Gustafsson, G.; Salaneck, W. R.; Osterholm, J. E.; Laakso, J. *Synth. Met.* **1989**, *28*, C377.
(104) Salaneck, W. R.; Inganas, O.; Nilsson, J. O.; Osterholm, J. E.; Themans, B.; Bredas, J. L. *Synth. Met.* **1989**, *28*, C451.
(105) Inganas, O.; Salaneck, W. R.; Osterholm, J. E.; Laakso, J. *Synth. Met.* **1988**, *22*, 395.
(106) Brown, S. P.; Spiess, H. W. *Chem. Rev.* **2001**, *101*, 4125.
(107) Opella, S. J.; Marassi, F. M. *Chem. Rev.* **2004**, *104*, 3587.
(108) Castellani, F.; van Rossum, B.; Diehl, A.; Schubert, M.; Rehbein, K.; Oschkinat, H. *Nature* **2002**, *420*, 98.
(109) Giessnerprettre, C.; Pullman, B.; Borer, P. N.; Kan, L. S.; Tso, P. O. P. *Biopolymers* **1976**, *15*, 2277.
(110) Yan, P.; Chowdhury, A.; Holman, M. W.; Adams, D. M. *J. Phys. Chem. B* **2005**, *109*, 724.
(111) Lahiri, S.; Thompson, J. L.; Moore, J. S. *J. Am. Chem. Soc.* **2000**, *122*, 11315.
(112) Justino, L. L. G.; Ramos, M. L.; Abreu, P. E.; Carvalho, R. A.; Sobral, A.; Scherf, U.; Burrows, H. D. *J. Phys. Chem. B* **2009**, *113*, 11808.
(113) Justino, L. L. G.; Ramos, M. L.; Knaapila, M.; Marques, A. T.; Kudla, C. J.; Scherf, U.; Almasy, L.; Schweins, R.; Burrows, H. D.; Monkman, A. P. *Macromolecules* **2011**, *44*, 334.
(114) Rahman, M. H.; Chen, H. L.; Chen, S. A.; Chu, P. P. J. *J. Chin. Chem. Soc.* **2010**, *57*, 490.
(115) Rahman, M. H.; Liao, S. C.; Chen, H. L.; Chen, J. H.; Ivanov, V. A.; Chu, P. P. J.; Chen, S. A. *Langmuir* **2009**, *25*, 1667.
(116) Le Bouch, N.; Auger, M.; Leclerc, M. *Macromol. Chem. Phys.* **2008**, *209*, 2455.
(117) Yazawa, K.; Inoue, Y.; Shimizu, T.; Tansho, M.; Asakawa, N. *J. Phys. Chem. B* **2010**, *114*, 1241.
(118) Tsao, H. N.; Cho, D. M.; Park, I.; Hansen, M. R.; Mavrinskiy, A.; Yoon, D. Y.; Graf, R.; Pisula, W.; Spiess, H. W.; Mullen, K. *J. Am. Chem. Soc.* **2011**, *133*, 2605.
(119) Gomes, J.; Mallion, R. B. *Chem. Rev.* **2001**, *101*, 1349.
(120) Johnson, C. E.; Bovey, F. A. *J. Chem. Phys.* **1958**, *29*, 1012.
(121) Schleyer, P. V.; Jiao, H. J. *Pure Appl. Chem.* **1996**, *68*, 209.
(122) Nakano, T.; Yade, T. *J. Am. Chem. Soc.* **2003**, *125*, 15474.
(123) Rathore, R.; Abdelwahed, S. H.; Guzei, I. A. *J. Am. Chem. Soc.* **2003**, *125*, 8712.
(124) Cheeseman, J. R.; Trucks, G. W.; Keith, T. A.; Frisch, M. J. *J. Chem. Phys.* **1996**, *104*, 5497.
(125) Spano, F. C. *Acc. Chem. Res.* **2010**, *43*, 429.
(126) Planken, K. L.; Colfen, H. *Nanoscale* **2010**, *2*, 1849.

(127) Cölfen, H. In *Analytical ultracentrifugation of colloids in Analytical Ultracentrifugation*; Scott, D. J., Harding, S. E., Rowe, A. J., Eds.; Royal Society of Chemistry: Cambridge, 2005; pp 501−583).
(128) Svedberg, T. *Kolloid-Z.* **1925**, *36*, 53.
(129) Svedberg, T. *Z. Phys. Chem.−Stochiom Verwandtschafts.* **1926**, *121*, 65.
(130) Schilling, K. Ph.D. Thesis, University Potsdam 1999.
(131) Svedberg, T.; Pedersen, K. O. *Angew. Chem., Steinkopff Verlag* **1940**, *53*, 195.
(132) Elias, H. G. *Makromoleküle*; Hüthig & Wepf: Basel, 1990.
(133) Schuck, P. *Biophys. J.* **2000**, *78*, 1606.
(134) Harding, S. E. *Biophys. Chem.* **1995**, *55*, 69.
(135) Berson, S.; De Bettignies, R.; Bailly, S.; Guillerez, S. *Adv. Funct. Mater.* **2007**, *17*, 1377.
(136) Pingel, P.; Zen, A.; Abellon, R. D.; Grozema, F. C.; Siebbeles, L. D. A.; Neher, D. *Adv. Funct. Mater.* **2010**, *20*, 2286.
(137) Brinkmann, M.; Rannou, P. *Macromolecules* **2009**, *42*, 1125.